HHS Public Access

Author manuscript

*Cancer Res*. Author manuscript; available in PMC 2017 March 15.

Published in final edited form as:

*Cancer Res*. 2016 March 15; 76(6): 1441–1450. doi:10.1158/0008-5472.CAN-15-1740.

# Detection of Pancreatic Cancer-induced Cachexia using a Fluorescent Myoblast Reporter System and Analysis of Metabolite Abundance

**Paul T. Winnard Jr.**[1], **Santosh Bharti**[1], **Marie-France Penet**[1,2], **Radharani Marik**[1], **Yelena Mironchik**[1], **Flonne Wildes**[1], **Anirban Maitra**[2,3], and **Zaver M. Bhujwalla**[1,2,*]

[1]Division of Cancer Imaging Research, The Russell H. Morgan Department of Radiology and Radiological Science, The Johns Hopkins University School of Medicine, Baltimore, MD, USA

[2]Sidney Kimmel Comprehensive Cancer Center, The Johns Hopkins University School of Medicine, Baltimore, MD, USA

[3]The University of Texas MD Anderson Cancer Center, TX, USA

## Abstract

The dire effects of cancer-induced cachexia undermine treatment and contribute to decreased survival rates. Therapeutic options for this syndrome are limited, and therefore efforts to identify signs of precachexia in cancer patients are necessary for early intervention. The applications of molecular and functional imaging that would enable a whole-body “holistic” approach to this problem may lead to new insights and advances for diagnosis and treatment of this syndrome. Here we have developed a myoblast optical reporter system with the purpose of identifying early cachectic events. We generated a myoblast cell line expressing a dual tdTomato:GFP construct that was grafted onto the muscle of mice bearing human pancreatic cancer xenografts to provide noninvasive live imaging of events associated with cancer-induced cachexia (i.e., weight loss). Real time optical imaging detected a strong tdTomato fluorescent signal from skeletal muscle grafts in mice with weight loses of only 1.2 to 2.7% and tumor burdens of only ~79 to ~170 $mm^3$. Weight loss in cachectic animals was also associated with a depletion of lipid, cholesterol, valine, and alanine levels, which may provide informative biomarkers of cachexia. Taken together, our findings demonstrate the utility of a reporter system that is capable of tracking tumor-induced weight loss, an early marker of cachexia. Future studies incorporating resected tissue from human pancreatic ductal adenocarcinoma (PDAC) into a reporter-carrying mouse may be able to provide a risk assessment of cachexia with possible implications for therapeutic development.

### Keywords

pancreatic cancer xenografts; cachexia; myoblast reporter; optical imaging; MR spectroscopy; plasma; muscle

[*]**Correspondence:** Zaver M. Bhujwalla, The Johns Hopkins University School of Medicine, The Russell H. Morgan Department of Radiology and Radiological Science, Division of Cancer Imaging Research, 720 Rutland Avenue, Rm 208C Traylor Building, Baltimore, MD, USA 21205, Office Phone: 410-955-9698, FAX: 410-614-1948, zaver@mri.jhu.edu.

**Conflict of Interest:** The authors have no potential conflicts of interest to disclose.

## Introduction

Cancer-induced cachexia occurs in several cancers and is a significant cause of morbidity and mortality (1–4). In pancreatic cancer, especially, the syndrome affects approximately 80% of patients (2). Cachexia compromises the effectiveness of cancer therapies, and contributes to decreased survival rates (1–6). An international effort has led to a more precise definition of cancer-associated cachexia and to objective measures of cachectic symptoms with the purpose of early diagnosis of the syndrome to achieve effective treatments (4). Cachexia is currently defined as an unintentional weight loss of >5% over a 6 month period, or a body-mass-index (BMI) <20kg/m$^2$ with ongoing weight loss of >2%, or sarcopenia and ongoing weight loss of >2% (4). Noninvasive biomarkers that identify precachectic patients who will progress to cachexia and refractory cachexia (4) are an urgent and unmet requirement. If the onset of cachexia is detected early, nutritional interventions appear to delay its progression (7). However, the systemic as well as molecular mechanisms initiating and driving cancer cachexia, as it presents in the clinic, have yet to be definitively identified and the syndrome remains an enigma even in the 21st century.

Despite extensive preclinical and clinical investigations into therapies aimed at reversing cachectic progression (7–10), to date only complete eradication of the cancer has been effective (1, 11). This is problematic as cachexia is most often recognized at later stages that include metastatic disease, where complete surgical resection of all malignant tissue is not feasible (12). Under these conditions, and independent of cancer type, it has been repeatedly demonstrated that cachexia is closely associated with increased co-morbidities, more complications during surgeries, less responsiveness to chemo- and radiotherapies, and thus, lower survival rates (1–3, 5, 11–13).

Transplantable tumor tissues or cell lines as well as carcinogen induced cancers have been extensively studied (14–18), and have provided important data strongly implicating hormones, cytokines, and catabolic pathways as contributing factors to cancer associated cachexia. However, mechanistic results with respect to causality of muscle specific wasting have often not been confirmed in clinical studies (19–26). Few rodent models of pancreatic cancer cachexia have been available, resulting in a sparse data set to draw conclusions from (15, 16). Moreover, currently there is no imaging reporter system for longitudinal monitoring to detect the early onset of this syndrome. The availability of such a reporter system in combination noninvasive metabolic imaging would allow the holistic identification of the temporal and spatial unfolding of metabolic patterns to obtain new insights into the cascade of metabolic events that drive the morbidity and mortality associated with this syndrome, identify new targets for its treatment, and identify clinically translatable biomarkers.

Here we report on the initial characterization of a myoblast optical imaging reporter that allowed real time longitudinal monitoring to detect the early onset of cancer induced wasting. The reporter myoblasts were engineered with inducible red fluorescence protein (tdTomato: tdT) expression driven by the human *muscle ring finger-1* (*MuRF1)* promoter, based on evidence that MuRF1 may be up-regulated during muscle atrophy (27). The myoblast reporter was validated in mice with human pancreatic cancer xenografts that

induced weight loss. We demonstrated that tdT fluorescence signals were reproducibly detected only from skeletal muscle grafts during weight loss and that tdT fluorescence could be quantified during small amounts of weight loss in mice with low tumor burdens. As a first step to holistically identifying the sequence of metabolic changes that occur with onset, quantitative $^{1}H$ magnetic resonance spectroscopy (MRS) of plasma identified a depletion of lipids, cholesterol and triacyglycerides (TAG) in lipoproteins, along with the ketone body precursor valine, as well as a reduction of alanine in the muscle of tumor bearing cachectic mice relative to tumor bearing weight gaining and non-tumor bearing control mice.

## Materials and Methods

### Generation of bidirectional dual reporter mammalian expression vector containing human *MuRF1* promoter

An in-house version of the pGL3basic (pGL3b) vector (Promega) was used as a backbone for the construction of our dual reporter vector. The tdT coding sequence (insert) was cloned into the luciferase site of our pGL3b vector using a Hind III plus Xba I digestion of the vector and insert followed by standard DNA purification and cloning steps generating pGL3b-tdT. A triple tandem (tT) glucocorticoid binding element (GRE) /FOXO1 binding element (FBE) sequence from the proximal promoter of the human *MuRF1* gene (27) gene fused to its core promoter sequence was synthesized at Biomatik and supplied as a pBlueScript construct. The promoter of pGL3b-tdT was excised with a Bsg I plus Kpn I digestion, blunted with T4 pol, and dephosphorylated with calf intestinal phosphatase (CIP). The tTMuRF1 promoter was excised from pBlueScript using Nhe I plus BamH I, filled-in with Klenow treatment, and cloned into pGL3b-tdT vector at the described Bsg I/Kpn I site generating pGL3b-tTMuRF1-tdT. An in-house pEF-1α-myc/his vector (Life Technologies) harboring a d2eGFP (Clonetech) cDNA was digested with Mlu I plus Alo I that released the entire EF-1α (promoter)-d2eGFP-BGH polyA expression cassette, which was blunted with Klenow. This insert was cloned at the Dra III site (T4 pol plus CIP treated) of pGL3b-tTMuRF1-tdT generating pGL3b-tTMuRF1-tdT:EF1α-eGFP. The orientation of the enhanced green fluorescent protein (eGFP) expression cassette was determined with appropriate restriction fragment analyses. The tTMuRF1 promoter sequence and a schematic representation of pGL3b-tTMuRF1-tdT:EF1α-eGFP are shown in Figure 1.

### Cell lines, cell culture, and myoblast differentiation conditions

Rat L6 myoblasts were obtained from ATCC in 2011. Human Panc1 (ATCC) and Pa04C cell lines (28, 29) were provided by Dr. Maitra of the Johns Hopkins University School of Medicine in 2012. The Panc1 cell line was established from a primary pancreatic ductal adenocarcinoma from a 56 year old male patient (30), and Pa04C was isolated from a lung metastasis in a 59 year old male patient with stage IV pancreatic adenocarcinoma (28). Panc1 and Pa04C were authenticated at the Johns Hopkins Genetic Resource Core Facility using human specific short tandem repeat (STR) markers, within the past six months. The STR profile of Panc1 and Pa04C cells were verified using the ATCC database. All cell lines were cultured in DMEM-10% FBS at standard 37° C, 5% $CO_2$, humidified incubator conditions.

Rat L6 cell cultures were initiated at 7,000 cells/$cm^2$ and maintained at ~40–50% confluence, to maintain their blast state. For differentiation, rat L6 cells were grown to ~90–100% confluence, then placed into DMEM-2% horse serum for 10–14 days and monitored visually for multinucleated myotube formation. Differentiation was considered complete when contraction of the fused myotubes away from small areas of the substratum was evident.

### Transfections and generation of stable cell lines

For myoblast transfection, DNA was mixed with Liptofectamine® 2000 reagent (Life Technologies) at a ratio of 1 μg DNA:3 μl Liptofectamine® 2000. DNA-Liptofectamine® 2000 mixtures were distributed onto L6 cells seeded 24 hr earlier onto wells of 6 well plates at 25,000 cells/well. After 24 hr the medium was changed and 72 hr later these were split and 1,000 cells of single-cell suspensions seeded onto 100 mm dishes. At the end of 2–3 weeks tdT fluorescence was induced with the addition of the synthetic glucocorticoid dexamethasone (DEX) to a final concentration of 1 μM and 24 hr later 12 of the brightest GFP/tdT positive colonies were selected and dispersed into wells of 6 well plates. After 4 days the cells were treated with DEX again. After 24 hr the dispersed expanded colonies contained 20–40% non-fluorescent cells. Pure stable clones exhibiting dual fluorescence were obtained by FACS at a Flow Cytometry Core Facility at the Johns Hopkins University School of Medicine. A bright fluorescence clone designated To3B was used throughout this study.

### Generation of subcutaneous (s.c.) tumor xenografts

All aseptic surgical procedures and animal handling were performed in accordance with protocols approved by the Johns Hopkins University Institutional Animal Care and Use Committee and conformed to the Guide for the Care and Use of Laboratory Animals published by the NIH. Six to eight week old severe combined immunodeficient (SCID) male mice were used in these studies. Panc1 or Pa04C cells ($5 \times 10^6$) in 50 μl of Hanks solution were injected into the right flank of mice.

### Mouse weights and tumor size measurements

Mice were weighed every 2–3 days. After the roughly ellipsoidal tumors became palpable, these were measured using a digital caliper at the time of weighing. Total tumor volumes ($mm^3$) were calculated as: Total Volume = 0.524(length × width × depth).

### Optical reporter L6 To3B muscle engraftment

The animals were split into two groups. The first group of two Panc1 and two Pa04C mice received To3B cell grafts 72 hr post *s.c.* injections of tumor cells, and were longitudinally evaluated over a 3 week tumor growth period. The second group of three Panc1 and two Pa04C mice received To3B cell grafts 4 days prior to sacrifice. At the time of inoculation of reporter cells, under 2.5% isoflurane/$O_2$ gas anesthesia, the fur was shaved and residual hair removed with NAIR® (Church & Dwight Co., Inc) from the right hind quarter of each mouse following which L6 To3B myoblasts ($2\times10^6$) in 50 μl of sterile Hanks were inoculated into the biceps femoris muscle region.

### Optical imaging and *ex vivo* microscopy

Live animal optical imaging of the muscle graft site was done using a Xenogen IVIS® Spectrum (PerkinElmer) optical scanner under 2.5% isoflurane/$O_2$ gas anesthesia. GFP signals were obtained with excitation/emission filter sets: 465nm/520nm, 465nm/540nm, and 500nm/540nm, while tdT fluorescence signals were obtained using an excitation filter of 570nm with emissions at: 620nm, 640nm, and 660nm. A 1 sec exposure was used for all imaging. Quantitative fluorescence intensities were acquired using Xenogen Living Image® 4.2 software package, with removal of background autofluorescence using the spectral unmixing tool followed by determination of regions-of-interest (ROIs) using the automatic ROI tool settings, which provided total quantitative fluorescence intensities from ROIs as Radiant Efficiencies with units of (photons/$cm^2$/sec/stradian) ÷ (μWatts/$cm^2$).

Phase contrast and fluorescence microscopy were done on a Nikon ECLIPSE TS 100 microscope (Nikon Instruments) equipped with a Photometrics CoolSnap ES digital camera (Roper Scientific) and FITC and Texas Red filter cubes. The fluorescence light source was an X-Cite 120 Fluorescence Illumination System (Photonic Solutions, Inc.). Muscle samples, dissected away from the bone following mouse euthanization, were opened along a ligament and placed flattened on a microscope slide. Images were obtained using a 2× objective, collected with NIS-Elements F3.2 software, and processed with ImageJ.

### Tissue processing

Tissue and plasma samples were obtained at the time of sacrifice on the final day of optical imaging. Mice were euthanized and the biceps femoris region of the left hind legs, *i.e.*, internal control skeletal muscle samples without the To3B myoblast grafts, were immediately cut away from the bone, snap frozen in liquid $N_2$, and stored at -80° C. Whole blood was collected by heart puncture into ice chilled EDTA-Vacuette tubes (Greiner Bio-One) and centrifuged at 2500×g for 10 min at 4° C. The plasma was decanted into fresh chilled cryotubes, and stored at -80° C. In addition, the biceps femoris muscle region with To3B grafts was cut away from the bone and placed in sterile PBS on ice until microscopic imaging that occurred within 15 min of dissection.

### $^1$H MRS analysis of plasma and muscle extracts

Plasma samples were thawed at room temperature, aliquots (100 μl) were mixed with 400 μL $D_2O$ (Deuterium Oxide, 99.8% D Atom), vortexed, and centrifuged at 5,000g for 5 min at 4° C. Supernatants (450 μL) were transferred into 5 mm NMR tubes for spectral acquisition. Wilmad Co-Axial stem inserts containing TSP (0.05% wt/vol in 50 μl $D_2O$) were used as the reference for quantitative analysis.

Snap frozen muscle samples (40 to 70 mg) were powdered under liquid nitrogen, weighed, and dual phase extraction was performed, as described previously (29). Samples were reconstituted in 500 μl of 1× phosphate buffered $D_2O$ (90% $D_2O$, 10% $H_2O$, pH = 7.4), vortexed, centrifuged at 500g for 5 min at 4° C, and supernatants (450 μL) were subjected for $^1$H MRS analysis. The lipid phase was evaporated to dryness under a stream of nitrogen, the residue was dissolved in 500 μl deuterated chloroform and methanol (2:1), and transferred to NMR tubes for spectral recordings.

Briefly, all $^{1}$H MR spectra were acquired at room temperature on an Avance III 750 MHz (17.6 T) Bruker MR spectrometer equipped with a 5 mm broad band inverse (BBI) probe. MR spectra of plasma, with water suppression achieved using presaturation, were acquired using a Carr-Purcell-Meiboom-Gill (CPMG) pulse sequence with a CMPG train of 100 $180^{0}$ pulses with 75 μs interpulse spacing (31, 32), with the following experimental parameters: spectral width of 15495.86 Hz, data points of 64 K, 90° flip angle, relaxation delay 6 sec, acquisition time 2.11 sec, 32 scans with 8 dummy scans, receiver gain 64 and spin echo time of 15 ms. For muscle extracts, aqueous and organic phase spectra were acquired using a single pulse sequence with 64 and 32 scans respectively, at a receiver gain of 128. All other acquisition parameters were the same as for plasma samples.

All spectral acquisition, processing and quantification were performed using TOPSPIN 2.1 software. Characterization of the metabolites was carried out on the basis of chemical shift, coupling constant, and splitting pattern of metabolites as reported in the literature and in comparison with standard MR spectra of metabolites from the Biological Magnetic Resonance Bank (31, 32). Area under peaks were integrated and normalized with respect to TSP and an unpaired Student *t*-test was performed.

## Results

### pGL3b-tTMuRF1-tdTomato:EF-1α-eGPF and evaluation of rat L6 To3B cells

A simplified schematic representation of the dual reporter vector is shown in Figure 1. The design of the inducible promoter was based on a triple-tandem repeat of the glucocorticoid response element-FOXO binding element (GRE-FBE) sequence and associated short flanking sequences from the proximal promoter region of the human *MuRF1* promoter (27) that was fused to the core promoter region (TATA box and transcription start site) of the same gene (Fig. 1A). Also included in the promoter is an additional FBE site that overlaps with the TATA box region, two putative SMAD binding elements (SBE), and possible myogenin binding elements (Fig. 1A). We have designated this promoter: tTMuRF1 (Fig. 1B). The schematic shown in Figure 1B indicates relative positions and orientations of all the basic components of the vector. We opted not to include a mammalian antibiotic selection marker as clone selections can be followed using GFP fluorescence.

As seen in Figure 1C at all stages of growth, including myoblasts at 40–50% confluence (top panel), myoblasts at 100% confluency (middle panel), and differentiated myotubes (bottom panel), red fluorescence was only observed after 24 hr of induction with DEX (+DEX) treatment.

To evaluate if To3B cells would exhibit constitutive tdT fluorescence activity, *i.e.*, leakiness, within the context of living muscle, we tested these reporter myoblasts as an orthotopic xenograft in the hind leg muscle of a normal nude mouse. During weekly imaging of GFP fluorescence to assess To3B graft growth, no tdT fluorescent signal was observed. At 4 weeks, *i.p.* administration of 100 μg DEX resulted in strong expression of tdT fluorescence at 24 hr (Supplemental Fig. S1). These data indicate that these L6 myoblast cells displayed stable constitutive expression of GFP, and inducible tdT fluorescence expression that was dependent on molecular events that occur in living muscle after an appropriate stimulus.

### Weight changes induced by human pancreatic cancer xenografts

In preliminary studies using an orthotopic model (Supplemental Material and Methods, Supplemental Fig. S2) we identified Pa04C tumors as inducing weight loss while mice with Panc1 tumors gained weight. Pa04C and Panc1 cell lines were therefore selected for *s.c.* implantation.

Figure 2A shows the weight changes in *s.c.* tumor bearing mice. Mice bearing Panc1 tumors gained weight while mice with Pa04C tumors lost weight throughout the duration of the study. The average change in weight between groups was significant ($*p \leq 0.05$) after 10 days of tumor growth (Fig. 2A). Mice bearing Pa04C tumors lost ~6 to 15% of their initial weight while, for comparison, animals with Panc1 tumors gained ~3 to 16% of their initial weight. Thus, weight loss or gain was dependent on the type of human pancreatic cells that the tumors were derived from.

### Optical imaging of To3B grafts in mice with human pancreatic cancer xenografts

As shown in Supplemental Figure S2B and S2C, we had preliminary evidence that tdT fluorescence was induced in weight losing mice. Hence, further optical imaging experiments were designed with two aims: 1) to test our ability to longitudinally track an early and persistent induction of tdT fluorescence, *i.e.*, the onset and chronic cachectic processes in muscle and 2) if that was not achieved, to track ongoing cachexia as induction of tdT during the 4 day period prior to sacrifice. Representative optical imaging of mice (numbered 1 & 2) bearing tumors of similar sizes are shown in Figure 2B. Robust GFP signals were recorded from the To3B graft site of these mice. Moreover, weight losing Pa04C mice exhibited strong tdT signals while little or no tdT signals were detected from weight gaining Panc1 mice (Fig. 2B) including those animals with tumors somewhat larger than Pa04C tumors.

We next sought *ex vivo* confirmation of the little or no induction of tdT fluorescence in To3B grafts from mice with Panc1 tumors. Microscopic images (Fig. 2C, 2× objective) showed that bright GFP fluorescence was seen from the To3B grafts in freshly dissected mouse hind legs from all mice. However, virtually no tdT fluorescence was detected from To3B grafts from mice with Panc1 tumors (Fig. 2C) while robust tdT fluorescence was readily seen in the grafts from mice with Pa04C tumors (Fig. 2C).

Figure 2D is a graphical representation of tdT/GFP signal ratios plotted against percent weight change. Figure 2D confirms that weight gain (Panc1 mice) was associated with low or zero tdT/GFP ratios while weight loss (Pa04C mice) was associated with high tdT/GFP ratios. During the longitudinal tracking of tdT expression, we observed tdT/GFP ratios above the background of ~0.25 at 8 and 10 days post Pa04C tumor cell inoculation (Supplemental Fig. S3) at which time small weight losses in the range of 1–2% were observed. These data suggest that the reporter system was detecting changes at low tumor burdens and small weight losses, indicative of early onset of cachexia. tdT/GFP ratios from Panc1 tumor bearing mice did not, at any time, exceed background levels of ~0.25.

Overall, the optical imaging data provided evidence that tdT fluorescence was switched on due to tumor associated changes that caused weight loss (Fig. 2D).

### Cachexia and tdT signal induction were independent of tumor size

Tumor growth curves are shown in Figure 3A. There was variation in the growth rate of Pa04C tumors (Fig. 3A). Two mice supported rapidly growing tumors while two supported slower tumor growth rates. Panc1 tumors grew at rates comparable to those of slow growing Pa04C tumors (Fig. 3A). All mice with Pa04C tumors were sacrificed after 22 or 24 days of tumor growth regardless of tumor size or growth rate (Fig. 3A), which proved to be independent of weight loss (Fig. 3B) as well as tdT fluorescence (Fig. 3C). To rule out the possibility that larger Panc1 tumor burdens would cause weight loss or would induce tdT fluorescence, three Panc1 mice were not sacrificed before their tumor sizes were at least comparable in size to those of the largest Pa04C tumors, *i.e.*, ≥ 400 $mm^3$, which occurred between 32 – 38 days after tumor cell inoculations (Fig. 3A). From Figure 3B it is seen that a small ~150 $mm^3$ Pa04C tumor could cause ~10% weight loss that was similar to mice with ~300 or 450 $mm^3$ Pa04C tumors. In comparison, ~50 to 500 $mm^3$ Panc1 tumor burdens correlated to weight gains only (Fig. 3B). Large Panc1 tumors did not exhibit corresponding proportional increases in tdT fluorescence. As shown in Figure 3C, tdT/GFP ratios across all Panc1 tumor sizes remained substantially lower than the tdT/GFP ratio of the smallest Pa04C tumor volumes.

### $^1$H MR spectroscopic analyses and quantifications of plasma and muscle metabolites

$^1$H MR spectroscopic analyses of plasma and muscle tissue obtained at the final imaging time point were used to determine differential metabolite changes in plasma (Figs. 4 and 5) and muscle (Fig. 6) from Pa04C mice as compared to normal and Panc1 mice. Representative $^1$H MR spectra of plasma obtained from Panc1, Pa04C, and normal mice are shown in Figure 4A. The representative differential changes in the lipid signal of lipoproteins from these three groups is evident in Figure 4A. A magnification of the appropriate spectral regions is shown in Figure 4B where the changes in TAG and cholesterol in the lipoproteins, and in valine are represented. Spectral analysis identified an ongoing depletion of these metabolites in the weight losing Pa04C mice and not in Panc1 tumor bearing mice. Quantification of the $^1$H MR plasma metabolites (Fig. 5A) indicated that lipids, cholesterol, TAG, and valine were significantly lower in plasma obtained from Pa04C tumor bearing mice compared to values in plasma of Panc1 tumor bearing mice and normal plasma ($^*p < 0.05$ and $^+p < 0.1$). Figure 5B indicates the positive correlation of decreases in plasma lipids, cholesterol, TAG, and valine levels with weight loss. Similarly, representative $^1$H MR spectra (Figure 6A) indicate a decrease of alanine in the muscle of Pa04C mice relative to the muscle obtained from Panc1 tumor bearing mice and normal mice. Quantification of these differences (Fig. 6B) indicates that alanine levels were significantly lower in muscle from Pa04C tumor bearing mice relative to normal and Panc1 tumor bearing mice ($^*p < 0.05$ and $^+p < 0.1$). As shown in Figure 6C, a strong positive correlation ($r^2 = 0.81$) was found between low muscle levels of alanine and weight loss.

## Discussion

Cancer associated cachexia is a multifactorial systemic condition. The resulting loss of lean muscle mass, compromises functional status, surgical outcomes, treatment strategies, and ultimately patient survival (1–5, 11, 12, 19–26). Lean skeletal muscle is the principal source

of protein for the body and the major integrated component of systemic protein, amino acid, and nitrogen homeostasis (6, 33, 34). Thus, cachexia reflects the depletion of protein reserves that initially spares protein in vital visceral organs, but ultimately results in a diminished, followed by a complete inability, to maintain normal vital functions.

The reporter system described here has the ability to noninvasively detect early onset of weight loss in living mice that can be combined with metabolic imaging using $^{1}$H MRS to holistically detect the cascade of metabolic changes that occur in normal tissues and organs with the onset of cachexia. The need to assess muscle loss over a time course of weeks has recently been underscored in a clinical longitudinal assessment of changes in skeletal muscle protein balance in weight losing upper GI tract cancer patients (10). In this first of its kind study, a higher fractional protein synthesis rate (FSR) of myofibrillar protein in weight losing cancer patients *vs* weight stable cancer patients and normal controls was observed unlike earlier clinical evaluations of lower FSRs in cachectic cancer patients. This discrepancy was suggested to be due to earlier studied FSR estimates being acquired over much shorter time courses of a few hours while the new approach encompassed a two week time period. A 2.9% increase of protein breakdown rate over FSR was found but an explanation was lacking as to how such a small increase could result in the large weight loss observed. Along these lines, our model system has the potential to investigate some of these unanswered questions.

The rationale for our selection of a *MuRF1*-based inducible promoter was based on evidence from cachectic rodent models that MuRF1, a muscle specific E3 ubiquitin ligase, was up regulated during muscle atrophy (27). An online search (see: www.gene-regulation.com) of our tTMuRF1 promoter sequence for putative *cis*-element binding factors revealed ~110 possible transcription factor binding sites including the myogenin and SMAD binding sites along with the GRE/FBE sites (Figure 1). SMADs and myogenin transcription factors have been associated with modulating skeletal muscle atrophy (35, 36) and moreover a pancreatic cancer cachexia clinical study has implicated the former (8). Numerous transcription factors are involved in the regulation of genes during normal homeostatic regulation of mature muscle mass and satellite cell regeneration (37, 38). Our reporter system was placed into skeletal muscle and hence subjected to similar complex genetic controls some of which may be revealed in future studies.

$^{1}$H MR spectral analyses of plasma and muscle metabolites provided corroborating evidence that cachectic subjects have disruptions in normal lipid and amino acid balances. The decrease in total lipid and TAG in the plasma lipoproteins of Pa04C mice as compared to normal and Panc1 mice likely reflects an increased lipid utilization, presumably from adipose stores, for energy production (fatty acid oxidation and gluconeogenesis from freed glycerol) after glycogen stores were depleted to conserve the body's protein reserves (39–41). The lower levels of total cholesterol found in plasma lipoproteins of Pa04C tumor bearing mice relative to normal and Panc1 tumor bearing mice indicates the loss of an important precursor used in hormone, bile acid, and vitamin D production. Cholesterol is a vital structural component of cell membranes and is involved in membrane associated signaling pathways. A lowering of plasma cholesterol may reflect a general compromise of cellular and systemic metabolic processes (42). A decrease in plasma valine, one of the

branched-chain amino acids (BCAA), in Pa04C tumor bearing mice may reflect a general decrease in BCAAs and, as a result, a lowered capacity to utilize important sources of ketone bodies (43) that act as alternative fuels during glucose reduction, especially for the maintenance of vital brain activity (44).

Alanine in muscle plays a role in balancing systemic glucose levels (9, 33, 34), and acts as a carrier of nitrogen (34) that may otherwise build up as toxic ammonia. Muscle released alanine is a substrate in liver for gluconeogenesis *via* pyruvate and the released nitrogen can be excreted as urea (34, 45). Alanine is also a stimulator of glucagon secretion from pancreatic alpha cells that further increases blood glucose levels (46). Given that insulin resistance is a common component of clinical cancer associated cachexia, it is possible that the lower alanine levels in muscle of Pa04C tumor bearing mice may be partly due to decreased glucose uptake and consequently, decreased pyruvate, the precursor of alanine (9). The decrease of alanine from cachectic muscle of Pa04C tumor bearing mice *vs* mice with Panc1 tumors or normal mice indicates that cachectic mice likely have a general lowered capacity to maintain normal systemic glucose hemostasis that is required for functioning of brain, erythrocytes, and immune cells. These $^{1}$H MR spectroscopic results provide new insights into metabolites that can be assessed clinically.

Importantly, we have shown the ability to distinguish between weight losing and weight gaining mice in the context of low tumor burdens. At sacrifice, tumor burdens were low and ranged from only 0.5 to 3% of body weight. At early time points during the longitudinal portion of the study we observed that very small Pa04C tumors; *e.g.*, ~79 to ~170 mm$^3$, induced tdT expression and provided above background fluorescence signals specific to small weight loss events of only 1.2 to 2.7% indicative of early onset of cachexia. This is a strong distinction between our model and previous cancer associated cachectic rodent models where generally very large tumor burdens of at least 10% of body weight and even tumor burdens of 30 – 40% of body weight have been common when studying cachexia (47, 48). Implanting inert “tumor” masses indicated that the mechanical burden of the tumor weight is a large contributing factor to the observed cachexia effects observed in some rodent models (47). Moreover, human tumor burdens rarely exceed 0.7% of body weight and as such our model may be a more accurate recapitulation of clinical observations (48).

In a recent report on a transgenic rat model, luciferase cDNA was knocked-in at the last intron of the *MuRF1* gene locus to regulate luciferase expression by the endogenous *MuRF1* promoter (49), but cancer induced wasting was not modeled. Modeling cancer cachexia on this Sprague-Dawley rat background will be limited to the few syngeneic tumor grafts that are known to generate cachexia or to carcinogenic induced cancer associated with cachexia in Sprague-Dawley rats (14, 15). Our relatively simple system offers greater flexibility and a similar capability of real-time optical monitoring of cachexia onset in tumor bearing animals.

We also have noted that the modeling of pancreatic cancer cachexia in rodents has been a challenge and very few reports are available resulting in a sparse dataset to draw conclusions from (15, 16). However, two recent reports on pancreatic cancer cachexia modeled in mice may contribute significant information in the future (43, 50). Our new reporter myoblast cell

line in the context of a *s.c.* pancreatic cancer xenograft model is, to the best of our knowledge, the first pancreatic cancer cachexia model system that is capable of longitudinally tracking cancer induced weight loss in mice.

Anorexia is often a contributing complication in clinical cancer cachexia, although caloric supplementation does not reverse the syndrome. Since we did not monitor food intake, decreased feeding could have contributed to weight loss. A resulting decrease in blood glucose levels may have been a contributing factor to the decreased alanine levels that we observed. We did detect early induction of tdT fluorescence in Pa04C tumor bearing mice at a time of insignificant weight loss suggesting that the reporter was activated prior to significant changes in weight loss. Future studies where weight loss is induced through a mechanism other than cancer will further evaluate the influence of weight loss on activating the reporter.

The work described here provides the groundwork for uncovering spatial and temporal changes in metabolism generated by the growing tumor that drive the initiation and consequences of cachexia. Such studies may also identify new targets in the treatment of this syndrome. The metabolic changes in plasma samples observed here require further validation in humans, and may provide a simple inexpensive assay to identify early onset.

## Supplementary Material

Refer to Web version on PubMed Central for supplementary material.

## Acknowledgements

We thank Mr. Gary Cromwell for inoculating the tumors.

**Grant Support:**

1. NIH R01 CA193365, P50 CA103175, R01 CA73850, R01 CA82337 to Z.M. Bhujwalla.
2. Cancer Functional Imaging Core support to Z. M. Bhujwalla from NIH P30 CA006973 to W. B. Nelson

## References

1. Theologides A. Cancer cachexia. Cancer. 1979; 43:2004–2012. [PubMed: 376104]
2. Utech AE, Tadros EM, Hayes TG, Garcia JM. Predicting survival in cancer patients: the role of cachexia and hormonal, nutritional and inflammatory markers. Journal of cachexia, sarcopenia and muscle. 2012; 3:245–251.
3. Dewys WD, Begg C, Lavin PT, Band PR, Bennett JM, Bertino JR, et al. Prognostic effect of weight loss prior to chemotherapy in cancer patients. Eastern Cooperative Oncology Group. The American journal of medicine. 1980; 69:491–497. [PubMed: 7424938]
4. Fearon K, Strasser F, Anker SD, Bosaeus I, Bruera E, Fainsinger RL, et al. Definition and classification of cancer cachexia: an international consensus. The Lancet Oncology. 2011; 12:489–495. [PubMed: 21296615]
5. Bachmann J, Buchler MW, Friess H, Martignoni ME. Cachexia in patients with chronic pancreatitis and pancreatic cancer: impact on survival and outcome. Nutrition and cancer. 2013; 65:827–833. [PubMed: 23909726]
6. Tsai S. Importance of lean body mass in the oncologic patient. Nutrition in clinical practice : official publication of the American Society for Parenteral and Enteral Nutrition. 2012; 27:593–598. [PubMed: 22898746]

7. Barber MD, Fearon KC, Tisdale MJ, McMillan DC, Ross JA. Effect of a fish oil-enriched nutritional supplement on metabolic mediators in patients with pancreatic cancer cachexia. Nutrition and cancer. 2001; 40:118–124. [PubMed: 11962246]
8. Johns N, Hatakeyama S, Stephens NA, Degen M, Degen S, Frieauff W, et al. Clinical classification of cancer cachexia: phenotypic correlates in human skeletal muscle. PloS one. 2014; 9:e83618. [PubMed: 24404136]
9. Lundholm K, Edstrom S, Ekman L, Karlberg I, Schersten T. Metabolism in peripheral tissues in cancer patients. Cancer treatment reports. 1981; 65(Suppl 5):79–83. [PubMed: 6809327]
10. MacDonald AJ, Johns N, Stephens NA, Greig CA, Ross JA, Small AC, et al. Habitual myofibrillar protein synthesis is normal in patients with upper GI cancer cachexia. Clinical cancer research : an official journal of the American Association for Cancer Research. 2014
11. Williams JP, Phillips BE, Smith K, Atherton PJ, Rankin D, Selby AL, et al. Effect of tumor burden and subsequent surgical resection on skeletal muscle mass and protein turnover in colorectal cancer patients. The American journal of clinical nutrition. 2012; 96:1064–1070. [PubMed: 23034966]
12. Bachmann J, Heiligensetzer M, Krakowski-Roosen H, Buchler MW, Friess H, Martignoni ME. Cachexia worsens prognosis in patients with resectable pancreatic cancer. J Gastrointest Surg. 2008; 12:1193–1201. [PubMed: 18347879]
13. Tan CR, Yaffee PM, Jamil LH, Lo SK, Nissen N, Pandol SJ, et al. Pancreatic cancer cachexia: a review of mechanisms and therapeutics. Front Physiol. 2014; 5:88. [PubMed: 24624094]
14. Honors MA, Kinzig KP. Characterization of the Yoshida sarcoma: a model of cancer cachexia. Supportive care in cancer : official journal of the Multinational Association of Supportive Care in Cancer. 2013; 21:2687–2694. [PubMed: 23689977]
15. Rivera JA, Graeme-Cook F, Werner J, Z'Graggen K, Rustgi AK, Rattner DW, et al. A rat model of pancreatic ductal adenocarcinoma: targeting chemical carcinogens. Surgery. 1997; 122:82–90. [PubMed: 9225919]
16. Tan MH, Shimano T, Chu TM. Differential localization of human pancreas cancer-associated antigen and carcinoembryonic antigen in homologous pancreatic tumoral xenograft. Journal of the National Cancer Institute. 1981; 67:563–569. [PubMed: 6944528]
17. Tanaka Y, Eda H, Tanaka T, Udagawa T, Ishikawa T, Horii I, et al. Experimental cancer cachexia induced by transplantable colon 26 adenocarcinoma in mice. Cancer research. 1990; 50:2290–2295. [PubMed: 2317817]
18. Tayek JA, Istfan NW, Jones CT, Hamawy KJ, Bistrian BR, Blackburn GL. Influence of the Walker 256 carcinosarcoma on muscle, tumor, and whole-body protein synthesis and growth rate in the cancer-bearing rat. Cancer research. 1986; 46:5649–5654. [PubMed: 3756911]
19. Dalal S, Hui D, Bidaut L, Lem K, Del Fabbro E, Crane C, et al. Relationships among body mass index, longitudinal body composition alterations, and survival in patients with locally advanced pancreatic cancer receiving chemoradiation: a pilot study. Journal of pain and symptom management. 2012; 44:181–191. [PubMed: 22695045]
20. D'Orlando C, Marzetti E, Francois S, Lorenzi M, Conti V, di Stasio E, et al. Gastric cancer does not affect the expression of atrophy-related genes in human skeletal muscle. Muscle & nerve. 2014; 49:528–533. [PubMed: 23835743]
21. Gallagher IJ, Stephens NA, MacDonald AJ, Skipworth RJ, Husi H, Greig CA, et al. Suppression of skeletal muscle turnover in cancer cachexia: evidence from the transcriptome in sequential human muscle biopsies. Clinical cancer research : an official journal of the American Association for Cancer Research. 2012; 18:2817–2827. [PubMed: 22452944]
22. Jagoe RT, Redfern CP, Roberts RG, Gibson GJ, Goodship TH. Skeletal muscle mRNA levels for cathepsin B, but not components of the ubiquitin-proteasome pathway, are increased in patients with lung cancer referred for thoracotomy. Clinical science. 2002; 102:353–361. [PubMed: 11869177]
23. Op den Kamp CM, Langen RC, Minnaard R, Kelders MC, Snepvangers FJ, Hesselink MK, et al. Pre-cachexia in patients with stages I-III non-small cell lung cancer: systemic inflammation and functional impairment without activation of skeletal muscle ubiquitin proteasome system. Lung Cancer. 2012; 76:112–117. [PubMed: 22018880]

24. Penna F, Costamagna D, Pin F, Camperi A, Fanzani A, Chiarpotto EM, et al. Autophagic degradation contributes to muscle wasting in cancer cachexia. The American journal of pathology. 2013; 182:1367–1378. [PubMed: 23395093]
25. Tardif N, Klaude M, Lundell L, Thorell A, Rooyackers O. Autophagic-lysosomal pathway is the main proteolytic system modified in the skeletal muscle of esophageal cancer patients. The American journal of clinical nutrition. 2013; 98:1485–1492. [PubMed: 24108784]
26. Wieland BM, Stewart GD, Skipworth RJ, Sangster K, Fearon KC, Ross JA, et al. Is there a human homologue to the murine proteolysis-inducing factor? Clinical cancer research : an official journal of the American Association for Cancer Research. 2007; 13:4984–4992. [PubMed: 17785548]
27. Waddell DS, Baehr LM, van den Brandt J, Johnsen SA, Reichardt HM, Furlow JD, et al. The glucocorticoid receptor and FOXO1 synergistically activate the skeletal muscle atrophy-associated MuRF1 gene. American journal of physiology Endocrinology and metabolism. 2008; 295:E785–E797. [PubMed: 18612045]
28. Jones S, Zhang X, Parsons DW, Lin JC, Leary RJ, Angenendt P, et al. Core signaling pathways in human pancreatic cancers revealed by global genomic analyses. Science. 2008; 321:1801–1806. [PubMed: 18772397]
29. Penet MF, Shah T, Bharti S, Krishnamachary B, Artemov D, Mironchik Y, et al. Metabolic Imaging of Pancreatic Ductal Adenocarcinoma Detects Altered Choline Metabolism. Clinical cancer research : an official journal of the American Association for Cancer Research. 2014
30. Lieber M, Mazzetta J, Nelson-Rees W, Kaplan M, Todaro G. Establishment of a continuous tumor-cell line (panc-1) from a human carcinoma of the exocrine pancreas. International journal of cancer Journal international du cancer. 1975; 15:741–747. [PubMed: 1140870]
31. Markley JL, Anderson ME, Cui Q, Eghbalnia HR, Lewis IA, Hegeman AD, et al. New bioinformatics resources for metabolomics. Pac Symp Biocomput. 2007:157–168. [PubMed: 17990489]
32. Bharti S, Roy R. Metabolite Identification in NMR-based Metabolomics. Current Metabolomics. 2014; 2:163–173.
33. Consoli A, Nurjhan N, Reilly JJ Jr, Bier DM, Gerich JE. Contribution of liver and skeletal muscle to alanine and lactate metabolism in humans. The American journal of physiology. 1990; 259:E677–E684. [PubMed: 2240206]
34. Felig P, Wahren J. Amino acid metabolism in exercising man. J Clin Invest. 1971; 50:2703–2714. [PubMed: 5129318]
35. Bollinger LM, Witczak CA, Houmard JA, Brault JJ. SMAD3 augments FoxO3-induced MuRF-1 promoter activity in a DNA-binding-dependent manner. American journal of physiology Cell physiology. 2014; 307:C278–C287. [PubMed: 24920680]
36. Macpherson PC, Wang X, Goldman D. Myogenin regulates denervation-dependent muscle atrophy in mouse soleus muscle. Journal of cellular biochemistry. 2011; 112:2149–2159. [PubMed: 21465538]
37. Cosgrove BD, Gilbert PM, Porpiglia E, Mourkioti F, Lee SP, Corbel SY, et al. Rejuvenation of the muscle stem cell population restores strength to injured aged muscles. Nature medicine. 2014; 20:255–264.
38. Scott IC, Tomlinson W, Walding A, Isherwood B, Dougall IG. Large-scale isolation of human skeletal muscle satellite cells from post-mortem tissue and development of quantitative assays to evaluate modulators of myogenesis. Journal of cachexia, sarcopenia and muscle. 2013; 4:157–169.
39. Hakvoort TB, Moerland PD, Frijters R, Sokolovic A, Labruyere WT, Vermeulen JL, et al. Interorgan coordination of the murine adaptive response to fasting. The Journal of biological chemistry. 2011; 286:16332–16343. [PubMed: 21393243]
40. Lowell BB, Goodman MN. Protein sparing in skeletal muscle during prolonged starvation. Dependence on lipid fuel availability. Diabetes. 1987; 36:14–19. [PubMed: 3792662]
41. Mallol R, Rodriguez MA, Brezmes J, Masana L, Correig X. Human serum/plasma lipoprotein analysis by NMR: application to the study of diabetic dyslipidemia. Prog Nucl Magn Reson Spectrosc. 2013; 70:1–24. [PubMed: 23540574]
42. Maxfield FR, Tabas I. Role of cholesterol and lipid organization in disease. Nature. 2005; 438:612–621. [PubMed: 16319881]

43. Shukla SK, Gebregiworgis T, Purohit V, Chaika NV, Gunda V, Radhakrishnan P, et al. Metabolic reprogramming induced by ketone bodies diminishes pancreatic cancer cachexia. Cancer & metabolism. 2014; 2:18. [PubMed: 25228990]
44. Owen OE, Morgan AP, Kemp HG, Sullivan JM, Herrera MG, Cahill GF Jr. Brain metabolism during fasting. J Clin Invest. 1967; 46:1589–1595. [PubMed: 6061736]
45. Leij-Halfwerk S, Dagnelie PC, van Den Berg JW, Wattimena JD, Hordijk-Luijk CH, Wilson JP. Weight loss and elevated gluconeogenesis from alanine in lung cancer patients. The American journal of clinical nutrition. 2000; 71:583–589. [PubMed: 10648275]
46. Muller WA, Faloona GR, Unger RH. The effect of alanine on glucagon secretion. J Clin Invest. 1971; 50:2215–2218. [PubMed: 5116210]
47. Morrison SD, Moley JF, Norton JA. Contribution of inert mass to experimental cancer cachexia in rats. Journal of the National Cancer Institute. 1984; 73:991–998. [PubMed: 6592392]
48. Pisters PW, Brennan MF. Amino acid metabolism in human cancer cachexia. Annual review of nutrition. 1990; 10:107–132.
49. Li W, Claypool MD, Friera AM, McLaughlin J, Baltgalvis KA, Smith IJ, et al. Noninvasive imaging of in vivo MuRF1 expression during muscle atrophy. PloS one. 2014; 9:e94032. [PubMed: 24710205]
50. Gilabert M, Calvo E, Airoldi A, Hamidi T, Moutardier V, Turrini O, et al. Pancreatic cancer-induced cachexia is Jak2-dependent in mice. Journal of cellular physiology. 2014; 229:1437–1443. [PubMed: 24648112]

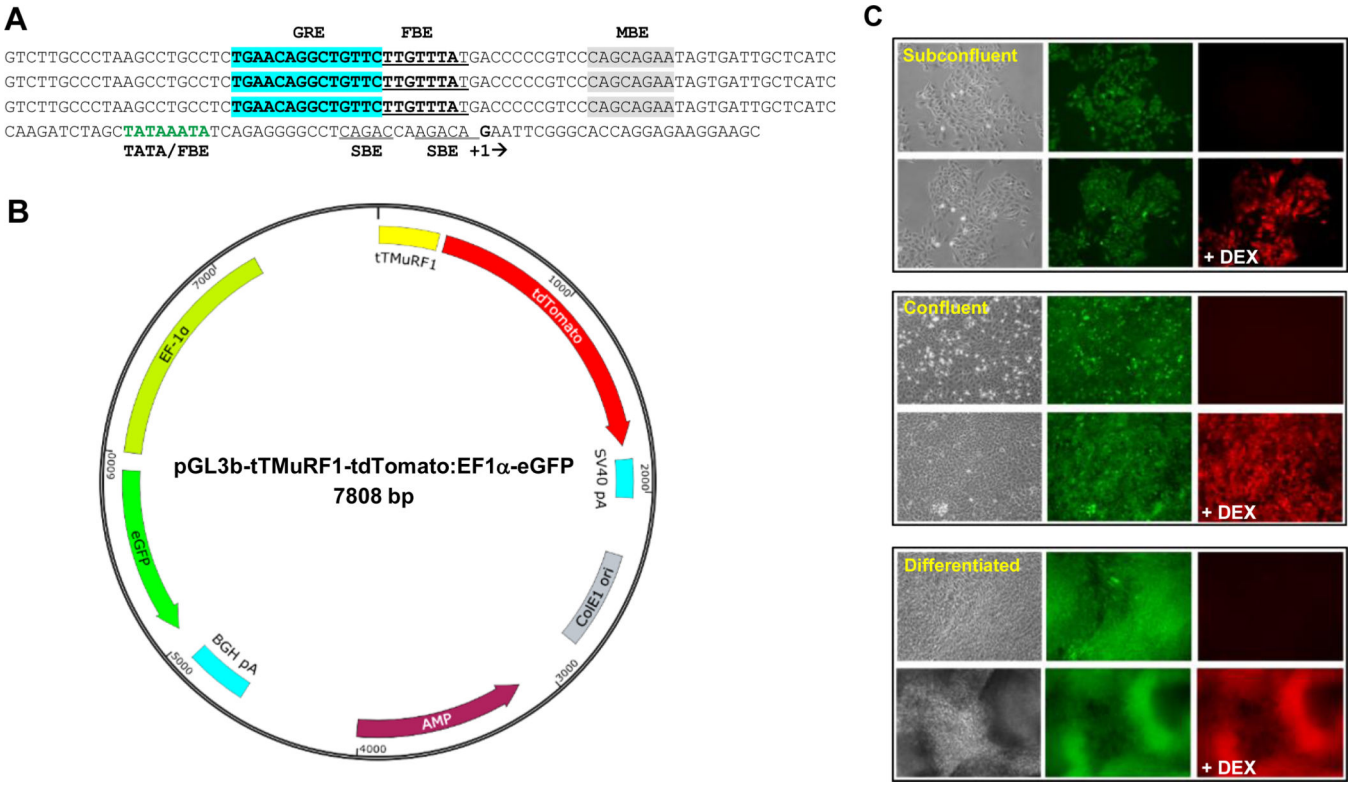


**Figure 1.**

Sequence of the tTMuRF1 promoter, schematic representation of pGL3b-tTMuRF1-tdT:EF1a-eGFP vector, and *in vitro* testing of To3B cells. (A) Triple tandem (tT) repeat of the sequence of a putative GRE-FBE (in bold-type and with GRE highlighted in blue) along with flanking sequence from the human *MuRF1* proximal promoter region fused to its core promoter, *i.e.*, the indicated TATA box that overlaps with another FBE (in green-type) with transcription start-site boxed (+1). SMAD binding elements (SBE, double underline) and putative myogenin binding element in gray highlight are also indicated. (B) Simplified schematic map of our dual reporter vector with tTMuRF1 promoter, tdTomato, simian virus 40 polyadenylation signal (SV40 polyA), EF1α promoter, eGFP, bovine growth hormone (BGH) polyA, ampicillin (AMP) resistance, and *E. coli* origin of replication (ColE1 ori) sequences mapped to their respective positions and orientations within the pGL3basic backbone. Note that this vector has no mammalian antibiotic selection marker. (C) Phase contrast and fluorescent microphotographs of To3B cells *in vitro* prior and 24 post dexamethasone (DEX) treatment. Three stages of cell growth are shown: subconfluent, confluent, and differentiated, in the top, middle, and bottom blocked images respectively. From the middle images of each block it is evident that To3B cells constitutively express GFP during all growth densities and at differentiation, which is independent of DEX treatment. The right-hand photos of each block of images show that tdT red fluorescence was only induced after DEX treatment (+DEX) and that this is the case for all growth densities as well as for differentiated myotubes. Images were obtained on an inverted microscope using a 20× objective and exposure times of 1 to 3 sec.

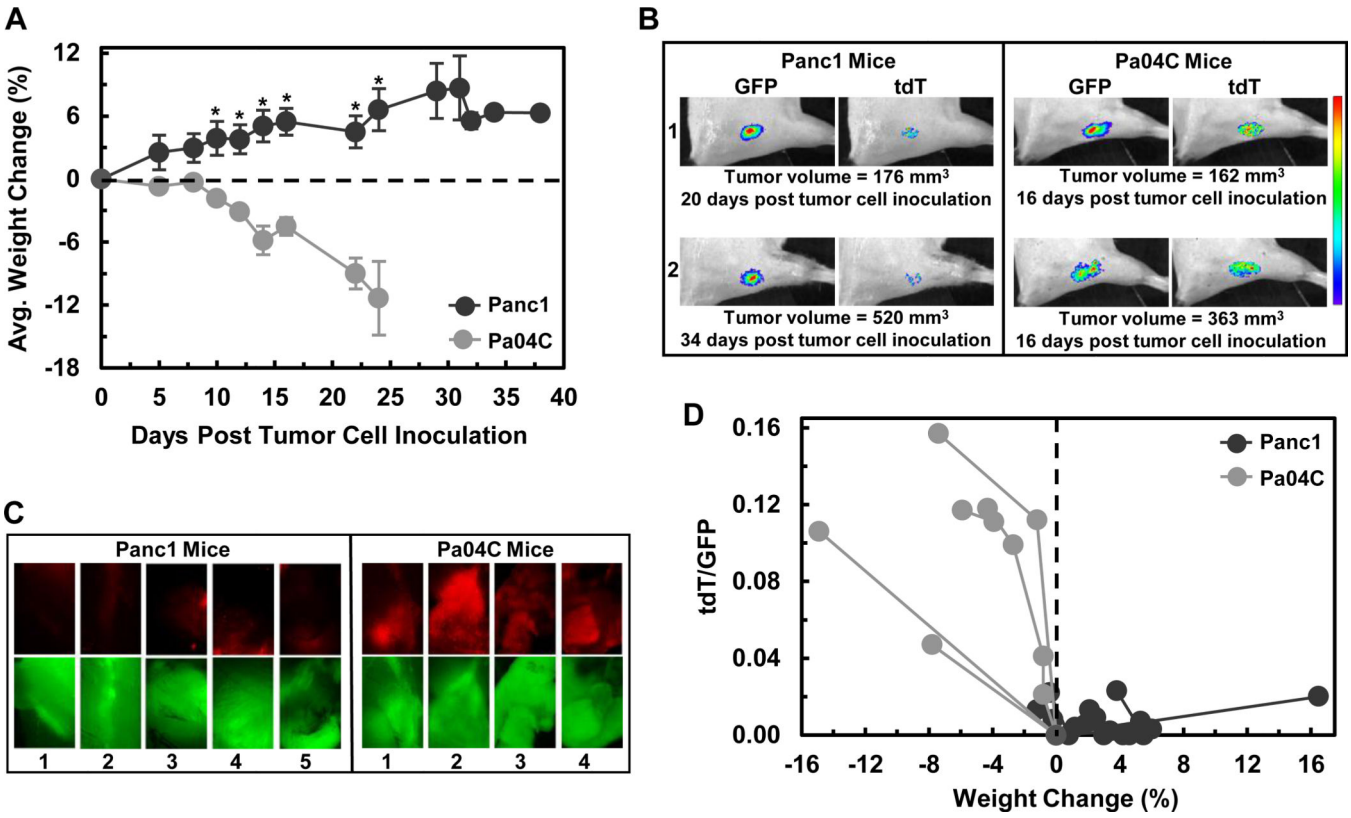


**Figure 2.**

Weight loss and induction of tdT fluorescence in To3B muscle grafts were pancreatic tumor cell line dependent. (A) Average magnitude of percent of weight changes for the 4 mice with Pa04C and 5 mice with Panc1 evaluated throughout the course of the study. The weight changes of mice with Panc1 tumors were significantly higher than mice with Pa04C tumors from day 10 onwards with $*p \leq 0.05$ (Student *t*-test). Error bars represent ±1 SEM. The last weight change of the remaining Panc1 mouse stands alone. (B) Representative GFP and tdT fluorescent images of To3B myoblast grafts of representative mice labeled 1 and 2 of each group. Note that the tumor sizes were similar and yet the tdT fluorescence from Panc1 tumor bearing mice was very low. Thus, a strong induction of tdT fluorescence was tumor type dependent. The heat map at the right is a qualitative presentation of fluorescent intensities that range from purple (dimmest) to red (brightest). All of the fluorescence areas represent quantifiable ROIs as automatically determined and evaluated in absolute units of total Radiance Efficency by Live Image® 4.2 software. (C) *Ex vivo* GFP and tdT fluorescent photomicrographs of To3B graft sites in dissected muscle. GFP fluorescence was recorded from To3B graft site of all Panc1 mice and Pa04C mice. Strong red tdT fluorescence was seen only in To3B grafts of Pa04C mice. Images were obtained on an inverted microscope using a 2× objective. (D) Graphical representation of tdT/GFP signal ratios *versus* percent weight changes. The tdT/GFP ratios for Panc1 mice were low or zero and clustered near or within the positive percent weight change region (weight gain) while tdT/GFP ratios of Pa04C mice were on average ~9× higher and were within the weight lost region.

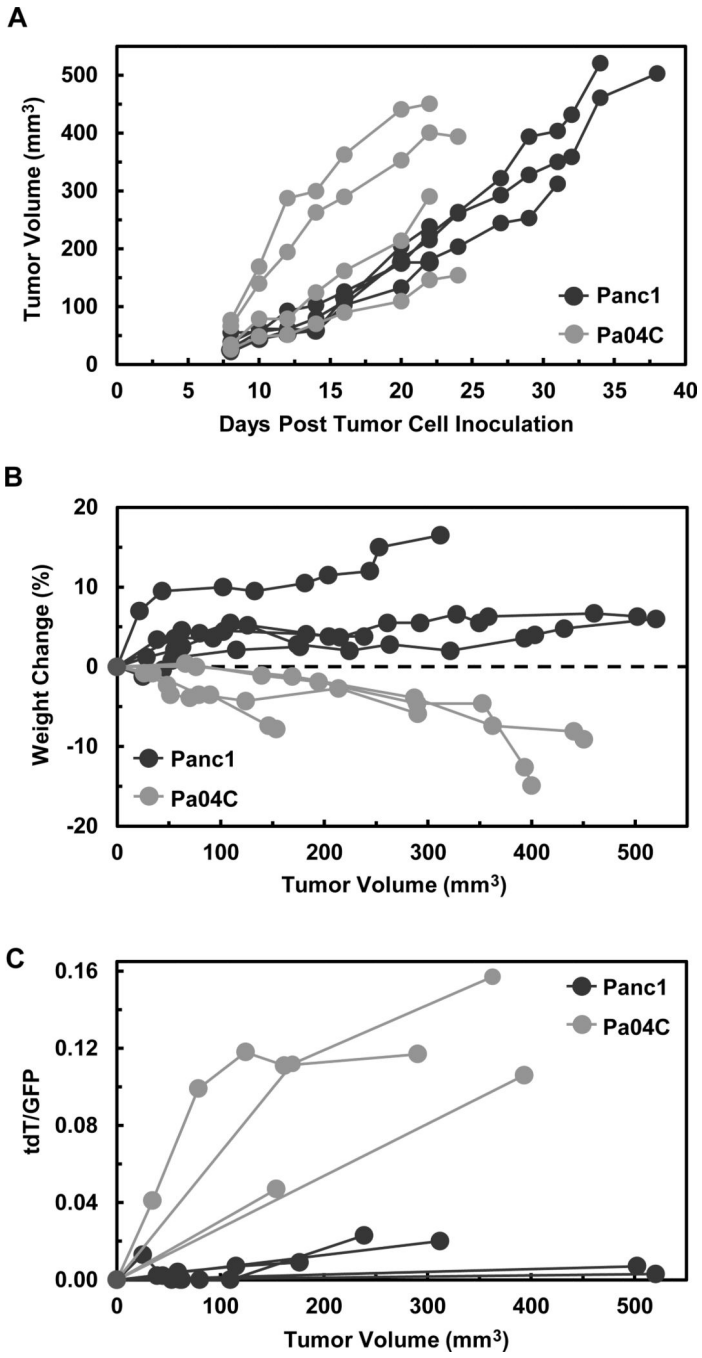


**Figure 3.**

Weight loss and induction of tdT fluorescence were directly associated with pancreatic tumor type but independent of tumor size. (A) Tumor volumes ($mm^3$) are presented for each mouse during the 24 days of tumor growth in Pa04C mice and 38 days of tumor growth in Panc1 mice. Tumor measurements were initiated 8 days after tumor cell inoculations. Tumor volumes = 0.524(L×W×D), *i.e.*, measured as ellipsoids with length, width, and depth. (B) Individual plots of percent weight change *vs* tumor size shows that across a range of sizes (~50 – 500 $mm^3$) all Panc1 mice gained weight while all Pa04C mice lost weight. (C)

tdT/GFP ratios plotted against tumor volumes shows that relatively high ratios were solely associated with Pa04C tumor bearing mice and lower tdT induction was characteristic of Panc1 tumor bearing mice including those with the largest tumor burdens.

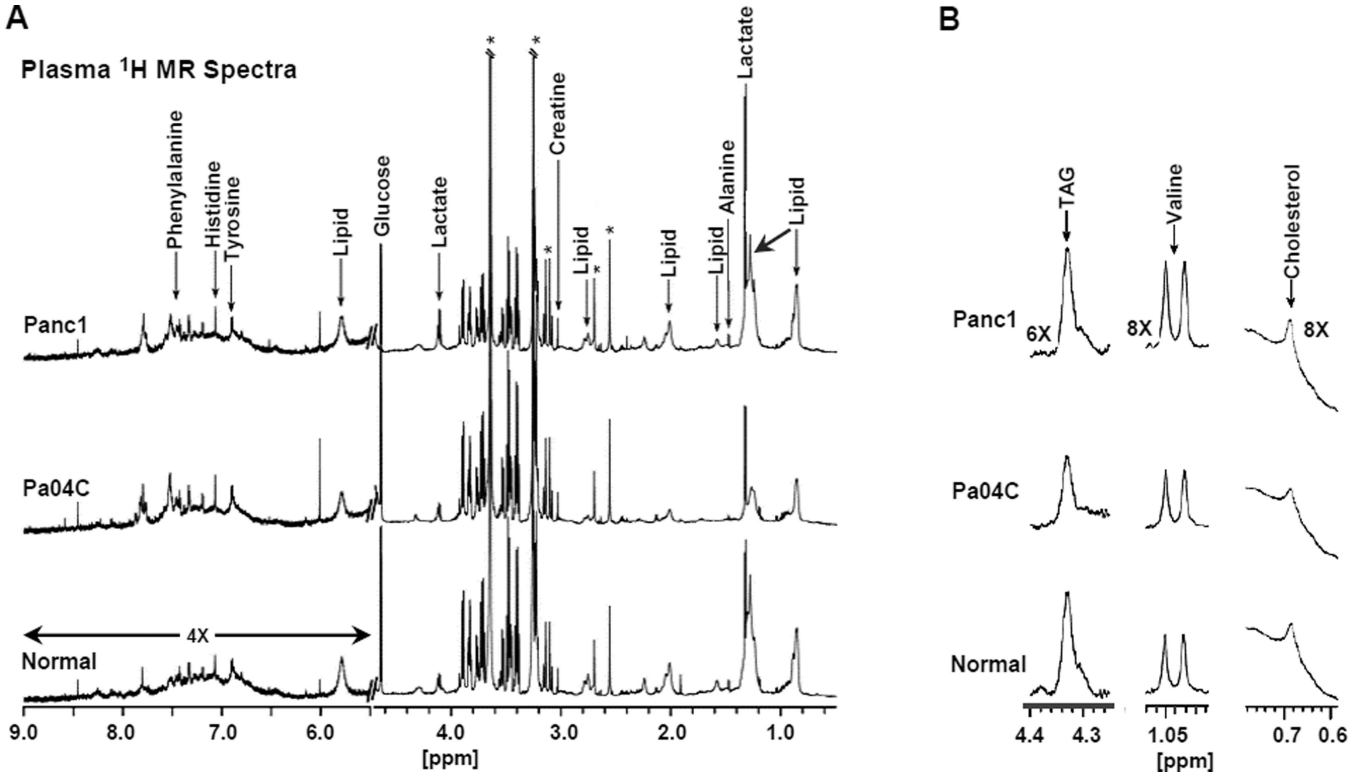


**Figure 4.**

$^{1}$H MR spectroscopic analysis of plasma samples from normal and Panc1 and Pa04C tumor bearing mice. (A) Typical pre-saturation water suppressed $^{1}$H CPMG MR spectra of mouse plasma. The CPMG sequence minimized the short $T_2$ signals from proteins. The downfield region (5.5 – 9.0 ppm) represents a 4× vertical zoom as compared to the up-field region (0.5 – 4.5 ppm). *Denotes signal from EDTA. (B) As indicated, 6× or 8× vertical zoom of the appropriate $^{1}$H MR spectral regions showing changes in plasma levels of TAG and cholesterol in lipoproteins, and in plasma levels of valine, in Pa04C, Panc1 tumor bearing mice, and normal mice.

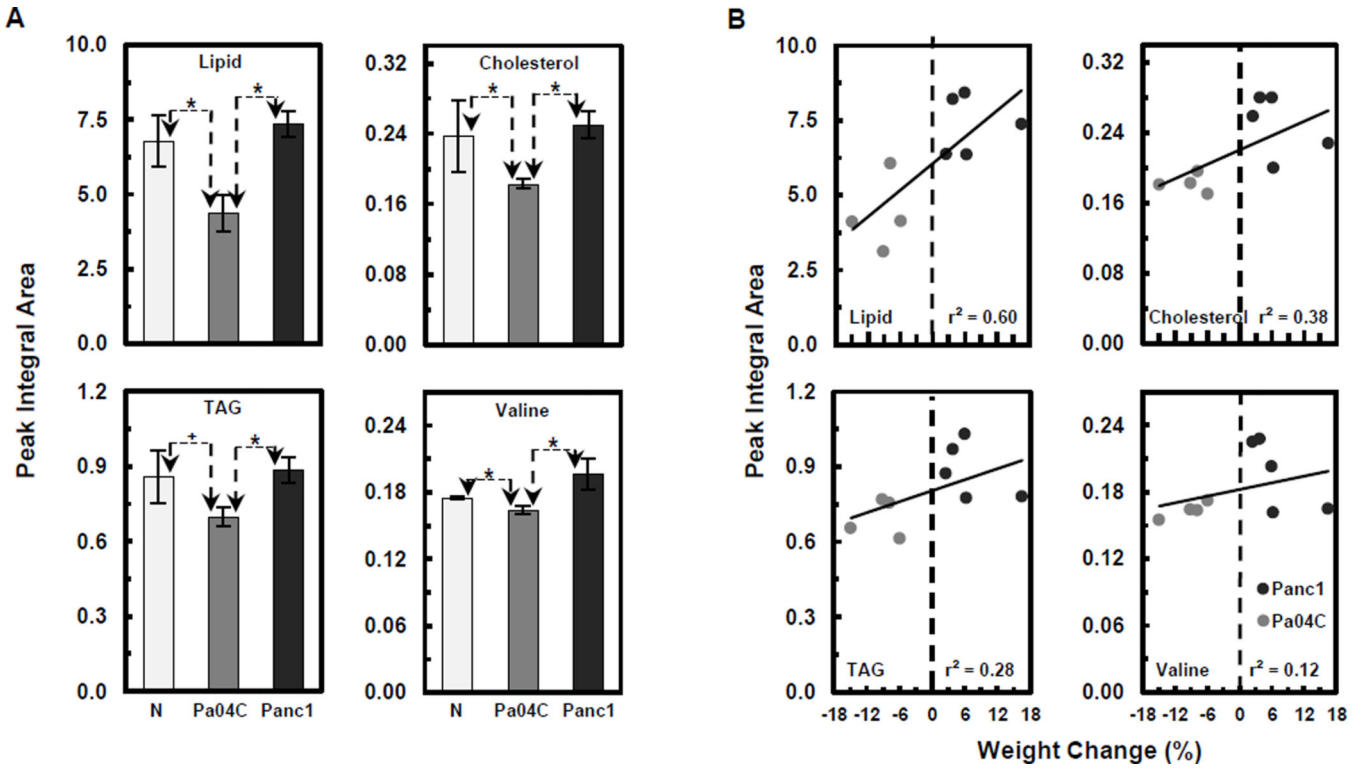


**Figure 5.**

Quantitative analysis and correlations of plasma metabolite losses to weight loss. (A) Bar graphs (integrations of peak areas) of lipids, cholesterol and TAG in lipoproteins, and valine, in normal (N), and Pa04C and Panc1 tumor bearing mice plasma. Significantly lower levels of each of these metabolites were observed in Pa04C plasma compared to normal or Panc1 plasma levels; $^{*}p \leq 0.05$, $^{+}p < 0.1$ (Students *t*-test). Error bars represent ±1 SEM. Peak integral areas (arbitrary unit) of lipids at 1.3 ppm, cholesterol at 0.68 ppm, TAG at 4.3 ppm, and valine at 1.05 ppm were used for quantification after normalization to the TSP reference. (B) Positive correlations of decreases in plasma lipids, cholesterol, TAG, and valine levels with degree of weight loss with coefficients of determination of: $r^2 = 0.60$, $r^2 = 0.38$, $r^2 = 0.28$, and $r^2 = 0.12$ respectively.

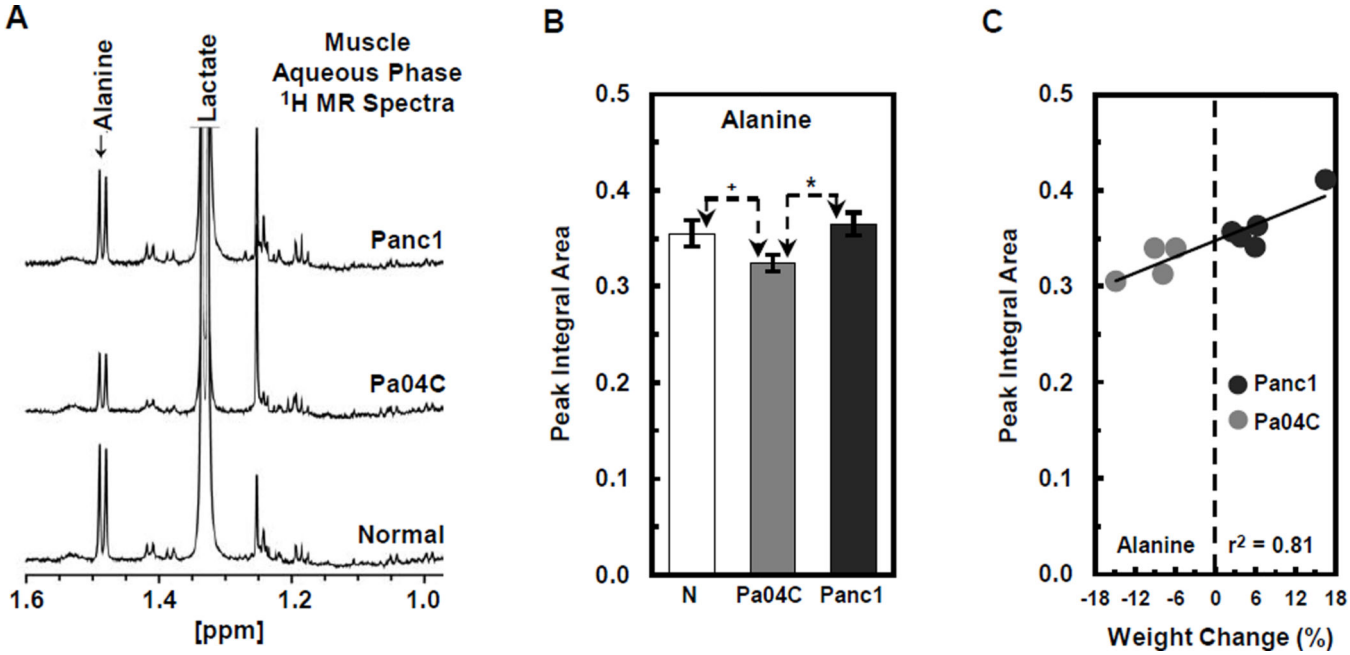


**Figure 6.**

$^{1}$H MR spectroscopic analysis and quantification of alanine levels in skeletal muscle from normal and Panc1 and Pa04C tumor bearing mice. (A) Representative $^{1}$H MR spectra indicate a decrease of alanine in the muscle of Pa04C mice relative to Panc1 and normal mice. (B) Quantification of these differences indicates that alanine levels were significantly lower in muscle from Pa04C tumor bearing mice relative to normal and Panc1 mice ($^{*}p < 0.05$ and $^{+}p < 0.1$). (C) A strong positive correlation ($r^2 = 0.81$) was found between low muscle levels of alanine and weight loss.